Properties and antioxidant activity of water-soluble iron catalysts with Schiff base ligands. Comparison with their manganese counterparts

Verónica A. Daier,[a] Claudia M. Palopoli,[a] Christelle Hureau,[b] Ariel De Candia,[c] and Sandra R. Signorella[a,*]

[a]*Facultad de Ciencias Bioquímicas y Farmacéuticas - Universidad Nacional de Rosario, IQUIR (Instituto de Química Rosario) - CONICET, Suipacha 531, S2002LRK Rosario, Argentina*
[b]*CNRS; LCC (Laboratoire de Chimie de Coordination); 205, route de Narbonne, F-31077 Toulouse, France and Université de Toulouse; UPS, INPT; LCC; F-31077 Toulouse, France*
[c]*Departamento de Química Inorgánica, Analítica y Química Física / INQUIMAE-CONICET, Facultad de Ciencias Exactas y Naturales, Universidad de Buenos Aires, Ciudad Universitaria, Pabellón 2, Buenos Aires, C1428EHA, Argentina*
E-mail: signorella@iquir-conicet.gov.ar

Dedicated to Professors Manuel González Sierra, Rita H. Rossi, Julio C. Podestá and Oscar S. Giordano for their outstanding contribution to the Organic Chemistry in Argentina

Abstract

Three new iron complexes $Na_2[Fe(5-SO_3-salpn)(H_2O)_2]OH \cdot 4H_2O$ (**1**$\cdot 4H_2O$), $Na_2[Fe(5-SO_3-salpnOH)(H_2O)_2]Cl \cdot 7H_2O$ (**2**$\cdot 7H_2O$) and $Na_2[Fe_2(5-SO_3-salpentO)(\mu-OAc)(\mu-(OH)(H_2O)_2]OH \cdot 3H_2O$ (**3**$\cdot 3H_2O$), where $5-SO_3$-salpn = 1,3-bis(5-SO$_3$-salicylidenamino)propane, $5-SO_3$-salpnOH = 1,3-bis(5-SO$_3$-salicylidenamino)propan-2-ol and $5-SO_3$-sapentOH = 1,5-bis(5-SO$_3$-salicylidenamino)pentan-3-ol, have been obtained and characterized. The ligands tune the redox potential of **1** and **2** within the range required for superoxide dismutase activity, with **2** being less reactive as a result of the formation of an inactive dimer. Complex **3** looses acetate and converts into a μ-oxo-Fe$_2$ species responsible for its catalase activity. The more negative reduction potentials of **1** – **3** and their lower stability result in rates of superoxide and peroxide disproportionation 10- to 100-times slower than those of the Mn counterparts.

Keywords: Water soluble Fe complexes, Schiff base ligands, antioxidant activity

Introduction

Peroxide and superoxide generated in the respiratory chain are usually well managed by aerobic organisms that employ superoxide dismutases (SODs) and catalases (CATs) to overcome the deleterious effects of these oxidants.[1,2] In many chronic inflammatory and degenerative diseases, the production of O_2^{2-} and $O_2^{\bullet-}$ is enhanced over the inactivating capability of CATs and SODs, thereby resulting in cell injury.[3] In this context, pharmacological research has pointed at the development of low molecular weight CAT and SOD mimics as therapeutic agents for the prevention of oxidative stress injuries. The active site of SODs may contain one penta-coordinated Fe or Mn ion in a N_3O_2 environment to dismutate $O_2^{\bullet-}$,[1] whereas CATs catalyze the disproportionation of H_2O_2 by using an Fe protoporphyrin IX or a bis(μ-oxo)(hydroxo)-μ-carboxylate dimanganese structural unit as the active site.[2] Therefore, to mimic these metallosites it is essential to employ ligands that reproduce the singularities of the metal environment in the biosite as well as the electronic properties that control catalysis.

To disproportionate $O_2^{\bullet-}$ and O_2^{2-} efficiently, the reduction potential of SOD and CAT is fine-tuned to values much lower than that of the $M^{3+}_{(ac)}/M^{2+}_{(ac)}$ couple.[4] However, in spite of the large number of Mn and Fe complexes that have shown CAT and/or SOD activity,[5,6] only a few studies have been performed on the ability of the ligand to control the redox potential and the divergence between Mn and Fe redox potentials in model compounds.[7] These aspects are essential for the rational design of more efficient catalytic antioxidants with improved stability under physiological conditions. In this context, we have synthesized, characterized and evaluated the electrochemical properties and SOD/CAT activity of water soluble mono- and dinuclear Fe complexes with the ligands: 1,3-bis(5-SO_3-salicylidenamino)propan-2-ol (5-SO_3-salpnOH), 1,3-bis(5-SO_3-salicylidenamino)propane (5-SO_3-salpn) and 1,5-bis(5-SO_3-salicylidenamino)pentan-3-ol (5-SO_3-salpentOH), and compared the redox properties and antioxidant activity of the new Fe complexes to those of the isostructural Mn counterparts.
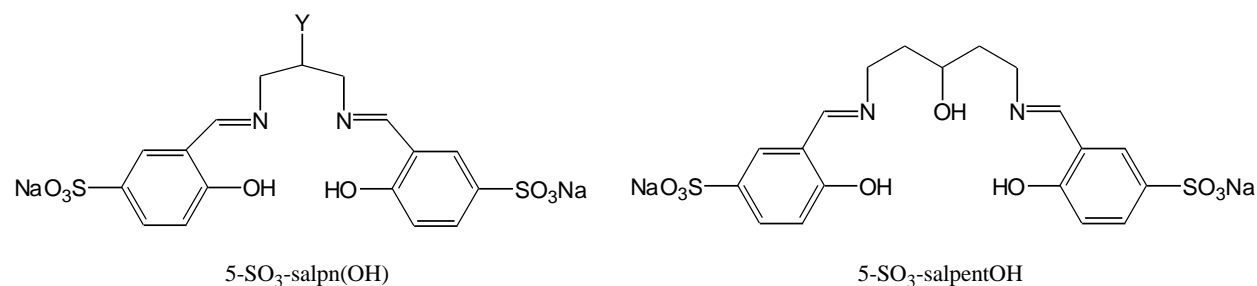

Figure 1. Ligands used in this work. Y = H in 5-SO_3-salpn and Y = OH in 5-SO_3-salpnOH.

Results and Discussion

Obtention and characterization of the catalysts
The three polydentate symmetric Schiff base ligands, 5-SO$_3$-salpnOH, 5-SO$_3$-salpn and 5-SO$_3$-salpentOH, were employed to prepare water soluble iron complexes of different nuclearity. While the length of the aliphatic chain between the imino groups in these ligands controlled the nuclearity of the resulting complex, introduction of -SO$_3^-$ as aromatic substituent led to complexes suitable for antioxidant activity studies in water solution. This is an important point, because most studied complexes are slightly soluble in water or lose activity under the conditions of antioxidant activity assays.[8]

Complexes Na$_2$[Fe(5-SO$_3$-salpn)(H$_2$O)$_2$]OH·4H$_2$O (**1**·4H$_2$O) and Na$_2$[Fe(5-SO$_3$-salpnOH)(H$_2$O)$_2$]Cl·7H$_2$O (**2**·7H$_2$O) were prepared from 1:1 mixtures of the ligand with FeCl$_3$ in methanol and the analytical results show that the two complexes retain two sodium ions per complex molecule in the solid state, but only complex **2** contains chloride. The IR spectra of **1 − 2** are very close (figure S1) and exhibit strong imine/phenolate absorptions at 1630-1623/1545-1538 cm^{-1} and two strong bands at 1110 and 1028 cm^{-1} attributable to the anti-symmetric and symmetric stretching modes of the -SO$_3^-$ groups. Comparison of the IR spectra of **1 − 2** with those of the well characterized Mn complexes formed with the same ligands[9] (figure 1S) evidences the "fingerprint" pattern of 5-SO$_3$-salpn and 5-SO$_3$-salpnOH coordinated to the metal and confirms the similar structures of Mn and Fe complexes obtained with the ligands acting through the N$_2$O$_2$ donor set.
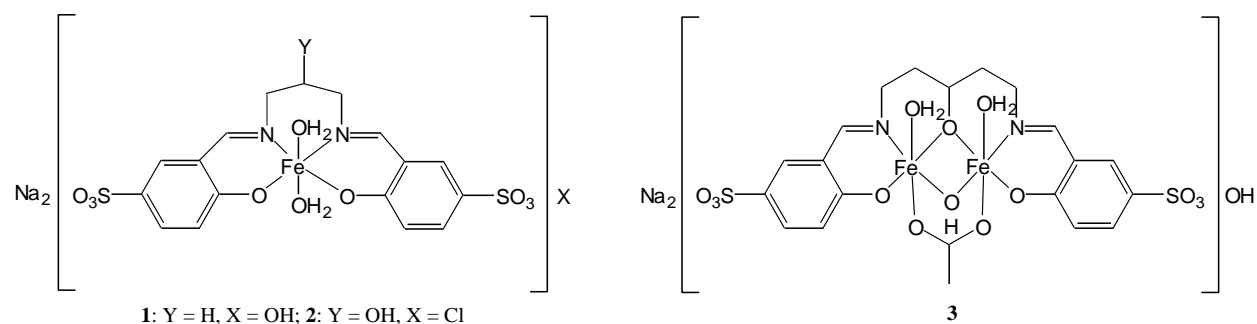

1: Y = H, X = OH; **2**: Y = OH, X = Cl   **3**

Figure 2. Complexes obtained with 5-SO$_3$-salpn, 5-SO$_3$-salpnOH and 5-SO$_3$-salpentOH.

The N$_2$O$_3$ pentadentate symmetric ligand, 5-SO$_3$-salpentOH, which provide an alkoxo oxygen for the endogenous bridging of two metal ions and two arms with N$_2$O$_2$ chelating donor sets, was reacted with 2 equivalents of Fe(OAc)$_2$ to afford the dinuclear Fe^{III} complex Na$_2$[Fe$_2$(5-SO$_3$-salpentO)(μ-OAc)(μ-OH)(H$_2$O)$_2$]OH·3H$_2$O (**3**·3H$_2$O). The IR spectrum of complex **3** (figure S2) exhibits strong imine and phenolate absorptions between 1635 and 1537 cm^{-1} that are shifted by ≈ 15 cm^{-1} from those in the free ligand due to the coordination of the metal to these groups and shows absorption peaks at 1552 cm^{-1} and 1427 cm^{-1}, that identify the anti-symmetric

and symmetric stretching vibrations of the *syn-syn* 1,3-bridging acetate.[10] The separation between the anti-symetric and symmetric absorptions ($\Delta \nu$) of 125 cm^{-1} is diagnostic of 1,3-bridging carboxylate.[10] The assignment was confirmed comparing the IR spectrum of **3** with those of Na$_2$[Fe$_2$(5-SO$_3$-salpentO)(μ-O)Cl(H$_2$O)][11] and Na[Mn$_2$(5-SO$_3$-salpentO)(μ-OAc)(μ-OMe)(H$_2$O)][12] (Figure S2). While bands characteristic of carboxylate stretching modes are absent in the IR spectrum of Na$_2$[Fe$_2$(5-SO$_3$-salpentO)(μ-O)Cl(H$_2$O)], complex **3** and the diMn complex show the two bands attributable to the bridging acetato anion separated by 125 cm^{-1}, indicating the same mode of bidentate acetato coordination in the two complexes.

Additionally, the IR spectra of compounds **1** – **3** display a broad band at $\approx$ 3400 cm^{-1} assigned to non-coordinated water molecules.

ESI-mass spectra of complexes **1** − **2** in methanol confirmed their chemical composition and showed that both complexes are mononuclear in solution. For complex **1**, the parent peak is observed at m/z = 494.1 (100%) in the negative mode ESI-mass spectra and originates from the [Fe(5-SO$_3$-salpn)]$^-$ monoanion. Two other minor peaks are also observed at m/z = 525 and 534 and correspond to the [Fe(5-SO$_3$-salpn)(OMe)]$^-$ and Na[Fe(5-SO$_3$-salpn)(OH)]$^-$ anions, respectively. In the case of complex **2**, solubility in methanol was not enough to give a good mass spectrum in the negative mode. Instead, in the positive mode ESI-mass spectrum two peaks at m/z = 563.7 and 585.7 could be observed, originated from the H$_2$[Fe(5-SO$_3$-salpnOH)(H$_2$O)-(MeOH)]$^+$ and NaH[Fe(5-SO$_3$-salpnOH)(MeOH)(H$_2$O)]$^+$ monocations.

The ESI-mass spectrum of **3** in methanol confirmed that dinuclearity of the complex is retained in solution. The negative mode mass spectrum of **3** is dominated by the peak at m/z = 683 corresponding to the monoanion [Fe$_2$(5-SO$_3$-salpentO)(MeO)(OAc)]$^-$, formed by replacement of hydroxide by methanolate originated from the solvent used in the spray experiments. Other minor peaks correspond to Na[Fe$_2$(5-SO$_3$-salpentO)(MeO)$_2$(OAc)]$^-$ (m/z = 737) and Na[Fe$_2$(5-SO$_3$-salpentO)(MeO)(OAc)$_2$]$^-$ (m/z = 765).

Electronic spectra of complexes **1** − **2** in aqueous solution consist of a broad band in the visible and a more intense band in the ultraviolet region (shown for **2** in figure 3(a)). The charge transfer (CT) bands from the phenolate to the metal have intermediate intensity, appear around 470 - 510 nm, and are responsible for the red color of these complexes. These transitions can be assigned to a charge transfer from the p$_\pi$ orbital of the phenolic oxygen to the d$_\pi$ orbital of the iron centre.[13] The similar spectral pattern of the electronic spectra of the two complexes is consistent with their analogous structure in solution.

The UV-vis spectrum of complex **3** (figure S3(a)) shows very strong electronic absorption bands in the UV and near-UV region (220-370 nm) and a less intense broad shoulder in the visible region (430-550). The absorption bands at 320 and 368 nm correspond to ligand-centered transitions overlapping with phenolate-to-metal charge-transfer ones. The broad shoulder in the visible region can be assigned as ligand field transitions whose unusually high intensities are due in part to the relaxation of spin restrictions upon antiferromagnetic coupling of the two iron atoms.[14]
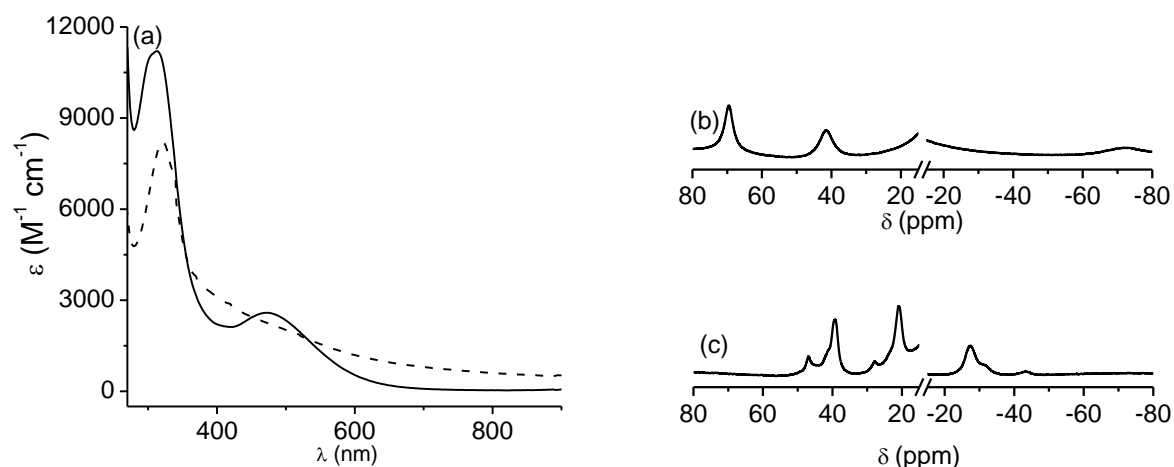
Figure 3. (a) Electronic spectra of aqueous solutions of **2** (▬) and **2** + 5 eq NaOH (---). (b) ^{1}H NMR spectra of **1** in D_2O. (c) ^{1}H NMR spectrum of **2** in phosphate buffer of pH 7.8 in D_2O.

Solutions of complexes **1 – 2** in D_2O, exhibit ^{1}H NMR spectra with features outside the diamagnetic region due to the presence of the S = 5/2 center, with a pattern of ring proton shifts consistent with dominant contact interactions that arise from the delocalization of unpaired spin density onto the symmetrically disposed ligand in the equatorial plane of the complex.[15] Previous NMR studies on Schiff base Fe^{III} complexes have shown that delocalization of unpaired spin density occurs via a π mechanism, resulting in an alternation in the sign of the contact shift exhibited by the protons of the phenolate moieties.[16] In the present case, the three resonances observed at 69.2, 41.3 and -71.9 ppm for **1** (shown in figure 3(b)) and 67.1, 46.5 and -71 ppm for **2**, can be assigned to H4/4', H6/6' and H3/3', respectively. Upon addition of base to an aqueous solution of complex **2**, resonances of the aromatic ring protons belonging to the original complex slowly disappear and are replaced by a larger number of resonances with lower contact shifts, indicating the starting complex transforms into another one in which the phenolate protons are not longer equivalent (figure 3(c)). In consonance with the decrease of chemical shifts in the paramagnetic NMR spectrum and the increasing number of resonances observed for the aromatic ring protons, the phenolate to Fe^{III} CT transition shifts to higher energy (figure 3(a)).[16b] This can be explained considering that in basic medium, deprotonation of the alcohol takes place and facilitates complex dimerization with the ligand acting through a N_2O_3 donor set. Such a behavior has previously been observed for metal complexes formed with salpnOH,[17] in which the ligand adopts an asymmetrical disposition around the metal. In this type of dimer, protons of the two phenol moieties are not longer equivalent and phenolate occupies equatorial and axial positions around iron and σ/π contact interactions should be operative. Besides, antiferromagnetic coupling of the two iron ions in the dimer should explain the smaller chemical shifts.[16a] The presence of a stronger axial ligand in the dimer is consistent with a ligand field increase that results in the blue shift of the CT band maxima, such as observed.[18]

The ^{1}H NMR spectrum of **3** in D$_4$-methanol is shown in figure 4(a). The spectrum is dominated by three broad resonances at 59.7, 38.6 and -57 ppm, assigned to the phenolate protons. This spectral pattern should result from a mechanism of π-spin delocalization through the C bonds of the two symmetrically related coordinated phenolate rings. Consequently, three resonances are expected from the two magnetically equivalent terminal phenolate ring protons with an alternating sign pattern of shifts in agreement with the π-spin-delocalization mechanism. The absence of the -105 ppm resonance in the spectrum of [Fe$_2$(5-SO$_3$-salpentO)(O)]$^-$ [11] (figure 4(b)) suggests this resonance can be assigned to the acetate methyl protons of **3**.

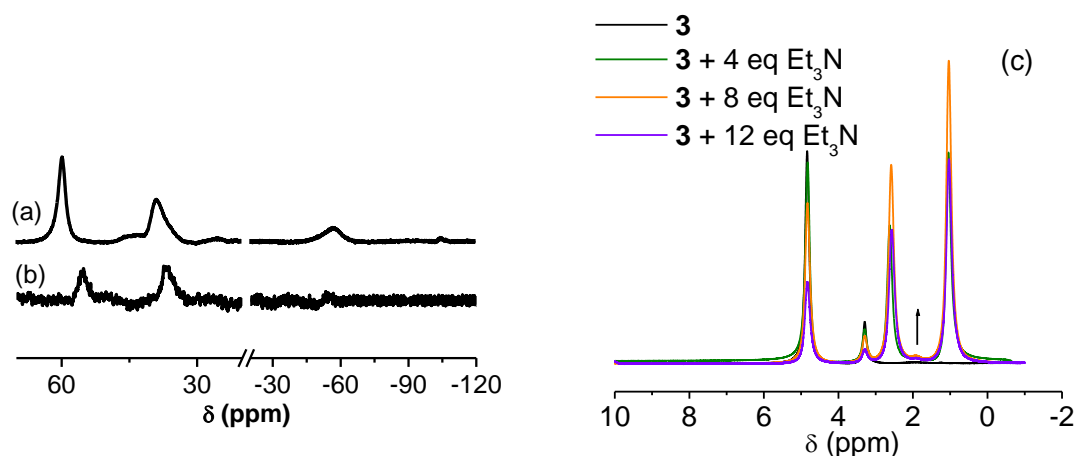**Figure 4.** Paramagnetic ^{1}H NMR spectra of **3** (a) and [Fe$_2$(5-SO$_3$-salpentO)(μ-O)]$^-$ (b) in D$_4$-methanol. Diamagnetic ^{1}H NMR spectra of **3** in D$_4$-methanol after addition of increasing amounts of Et$_3$N (c).

Addition of Et$_3$N to the methanol solution of **3** results in paramagnetic spectra with smaller chemical shifts. The spectral changes caused by the basic medium suggests conversion of the starting complex into a μ-oxo one in which antiferromagnetic coupling of the two iron ions is favored. Inspection of the diamagnetic region after addition of Et$_3$N shows the appearance of the free acetate resonance at 1.9 ppm (figure 4(c)). The intensity of the acetate peak increases with increasing amounts of Et$_3$N, thus implying that conversion into the μ-oxo complex involves acetate dissociation. Electronic spectroscopy provided another piece of evidence supporting conversion into the μ-oxo complex. UV-vis spectra of solutions of complex **3** + Et$_3$N showed that the band at 320 nm shifts to 368 nm and its intensity increases after addition of Et$_3$N (figure S3(a)). Apparition of the red shifted band is concurrent with the decrease of the absorbance at 320 nm and occurs with an isosbestic point at 335 nm, indicating direct conversion of the initial complex into a new species. The band at 368 nm may correspond to oxo to Fe^{III} CT transitions through π overlap between p orbitals of the oxo group and d orbitals on the iron.[19] In complex **3**,

these transitions are superimposed on intraligand transitions of the sulphonato ligand and phenolate to Fe^{III} CT transitions.

Electrochemistry and antioxidant activity of complexes (1 – 3)

Aqueous solutions of complexes **1 – 2** display in cyclic voltammetry a single quasi-reversible redox process at -0.18 and -0.15 V, respectively, attributable to the Fe^{III}/Fe^{II} couple, which was confirmed by voltammetry at a rotating electrode. These reduction potentials are in accordance with similar values found for the four-coordinate Fe-salen complex.[16b] At variance, it has been found that for five-coordinate Fe-salen-L (salen = 1,2-bis(salicylidenamino)ethane; L = anionic ligand) that contain one additional anion bound to Fe, the potentials of the Fe^{III}/Fe^{II} couples are shifted to much lower values associated with the change in the donor set around Fe.[20] Therefore, the electrochemical results confirm that both 5-SO_3-salpn and 5-SO_3-salpnOH bind Fe through the N_2O_2 donor set. The reduction potentials of the Fe complexes are 0.1 V more negative than the structurally analogue Mn complexes, [Mn(5-SO_3-salpn)]$^-$ and [Mn(5-SO_3-salpnOH)]$^-$.[9] This ΔE(Fe/Mn) is lower than observed for five- and six-coordinate isoestructural Fe/Mn compounds with high proportion of N-donor sites in the coordination sphere, for which ΔE(Fe/Mn) values were found in the 0.25 to 0.55 V range in CH_3CN.[7] The low ΔE(Fe/Mn) found for the Fe/Mn complexes of 5-SO_3-salpn and 5-SO_3-salpnOH is consistent with the fact that ΔE(Fe/Mn) tends to decrease with the increase of the O/N ratio in the metal coordination sphere.

In methanol, the cyclic voltammogram of complex **3** showed two quasi-reversible reductions at 0.04 and -0.35 V (*vs* Ag/AgCl), corresponding to the $Fe^{III}_2/Fe^{III}Fe^{II}$ and $Fe^{III}Fe^{II}/Fe^{II}_2$ redox couples, which were confirmed by voltammetry at a rotating electrode. The potential of the first one-electron reduction of **3** results to be 0.11 V more negative than found for the diMn counterpart.[12] Thus, ΔE(Fe/Mn) is similar as found for mononuclear complexes described above, and indicate that the general trend is still valid for dinuclear Fe_2/Mn_2 complexes: "lower potentials for the Fe counterparts and low ΔE(Fe/Mn) for complexes with O-rich coordination sphere". Upon addition of Et_3N to the methanol solution of **3** the cyclic voltammogram showed an irreversible reduction at -0.76 V (vs Ag/AgCl), corresponding to the Fe^{III}_2/Fe^{II}_2 couple. Linear voltammetry confirmed this process can be assigned to a two-electron reduction. The shift of the Fe^{III}_2/Fe^{II}_2 couple to lower potentials in basic medium is consistent with the conversion of the starting complex into the μ-oxo-Fe_2 complex.[19]

SOD activity studies

The Fe^{III}/Fe^{II} redox couples of **1** and **2** are within the potential range -0.4 V ($O_2/O_2^{\bullet-}$) to 0.65 V ($O_2^{\bullet-}/H_2O_2$). Therefore, these complexes are expected to exhibit SOD activity. The activity of complexes **1 – 2** toward superoxide in aqueous buffer was evaluated by using the nitro blue tetrazolium (NBT) assay. This assay is based on kinetic competition for the superoxide reaction between NBT and the complex with SOD activity. In this way, the SOD activity is inversely related to the amount of formazan, the purple product formed by reaction of NBT with superoxide, observed at 560 nm. Both **1** and **2** were found to inhibit the reduction of NBT, as shown in Figure

5. Inhibition percentages were measured for several complex concentrations and the IC_{50} values were 6.2 μM **1** and 14 μM **2**. The lower SOD activity of **2** should be the consequence of dimerization of this complex in the basic medium, initiated by deprotonation of the OH group on C2 of the propane backbone of the ligand, just as described in the previous section. Dimers are not suitable to mimic SODs, which dismutate $O_2^{\bullet-}$ at an active site containing one metal ion in a N_3O_2 environment; and this is especially evident for electronically coupled dimetal centers that are usually involved in catalysis of two-electron redox reactions. In figure 5, the SOD activity of complexes **1** − **2** is compared to that of the water soluble Mn analogues, [Mn(5-SO$_3$-salpn(OH))]$^-$. These complexes show Mn^{III}/Mn^{II} couples at -0.08 and -0.05 V, and the IC_{50} values, measured under the same experimental conditions as complexes **1** − **2**, were 0.77 and 1.14 μM. These IC_{50} values are one order of magnitude lower than for the Fe analogues, a fact consistent with the observation that the catalytic rate constants for dismutation of the superoxide anion are related to the metal-centered reduction potential of the catalysts.[21] Therefore, the more potent mimics are those whose M^{III}/M^{II} couple are closer to the midpoint potential between the reduction and oxidation of $O_2^{\bullet-}$ ($E_{1/2}$ 0.12 V vs. Ag/AgCl).
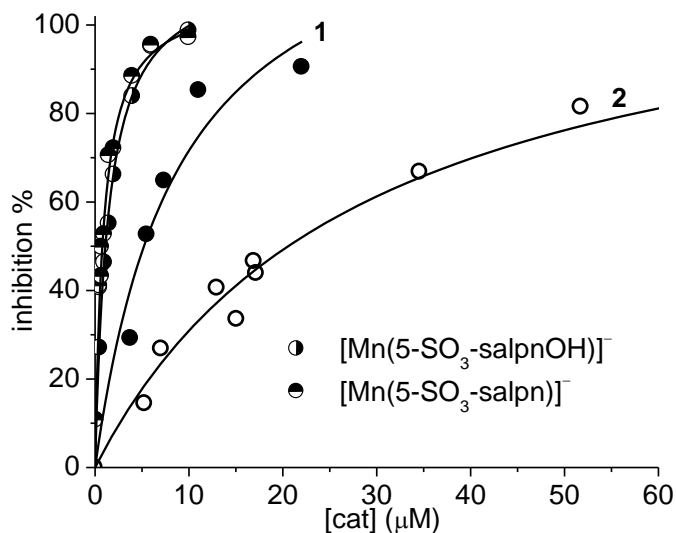

Figure 5. SOD-activity of complexes **1** and **2** and their Mn analogues in the riboflavin-methionine-NBT assay.

To disproportionate $O_2^{\bullet-}$ efficiently, the reduction potentials of FeSOD and MnSOD are fine-tuned to -0.02 and 0.05 V, respectively.[4] These values are much lower than those of the $M^{3+}_{(ac)}/M^{2+}_{(ac)}$ couples: $Fe^{3+}_{(ac)}/Fe^{2+}_{(ac)} = 0.53$ V and $Mn^{3+}_{(ac)}/Mn^{2+}_{(ac)} = 1.3$ V. Despite the metal active sites of FeSOD and MnSOD have been proven to be structurally identical, FeSOD and their MnSOD analogues are inactive when substituted with Mn (Fe) as a result of the shift in the redox potentials upon substitution. The reduction potential of the Fe substituted MnSOD

decreases to -0.48 V, while that of the Mn substituted FeSOD increases to 0.66 V,[22] and these values are out of the range required for SOD activity. In the case of Fe/Mn-salpn(OH) mimics, ΔE(Fe/Mn) of 0.11 V reduces k_{cat} from 2.4 – 3.6 x 10^6 M^{-1} s^{-1} for the Mn complexes to 1.96 – 4.4 $\times 10^5$ M^{-1} s^{-1} for the Fe analogues. For the active site of SOD, which contains a N_3O_2 donor set, the expected ΔE(Fe/Mn) based on first sphere effects only, should be between 0.11 (N_2O_2, present study) and 0.45 V (N_4O_2[7b]). These facts support the idea that primary ligand sphere in Fe and MnSODs should render both metal ions competent to carry out the enzymatic reaction and that it is the more distant electrostatic contributions that may be the source of metal-specific activity.[7a]

CAT activity studies

Catalase enzymes disproportionate hydrogen peroxide by converting it into water and oxygen. While FeCATs are heme-proteins that dismutate H_2O_2 employing $Fe^{III}/Fe^{IV}=O^{\bullet+}$, MnCATs possess a $Mn_2(\mu\text{-}O_2CR)(\mu\text{-}O/OH)_2$ structural unit as the active site that cycles between the Mn^{II}_2 and Mn^{III}_2 oxidation states during catalysis.[2] To act as CAT mimics, synthetic catalysts must have metal centered redox couples within the 0.04 V (O_2/H_2O_2) to 1.01 V (H_2O/H_2O_2) potential range. A number of dinuclear manganese-based complexes has been investigated as low molecular weight catalytic scavengers of H_2O_2.[5b-d] Among them, the complex [$Mn_2(5\text{-}SO_3\text{-}salpentO)(\mu\text{-}OAc)(OMe)$]$^-$ has shown to be highly efficient to dismutate H_2O_2 in basic aqueous solution, where the complex converts into [$Mn_2(5\text{-}SO_3\text{-}salpentO)(\mu\text{-}O)$]$^-$.[12] $Fe_2(\mu\text{-}O_2CR)_{1(2)}(\mu\text{-}O(R))$ centers are ubiquitous in biology, occurring in oxygen transport proteins, ribonucleotide reductases, purple acid phosphatases, methane monooxygenase, among others, but are not involved in CAT activity.[23] To extend the analysis of the effect of the ligand on redox properties and activity of Fe/Mn analogues to dinuclear complexes, we decided to evaluate the CAT activity of **3**, and compare it to that of [$Mn_2(5\text{-}SO_3\text{-}salpentO)(\mu\text{-}OAc)(\mu\text{-}OMe)$]$^-$ and [$Mn_2(5\text{-}SO_3\text{-}salpentO)(\mu\text{-}O)$]$^-$.

　　　To disproportionate H_2O_2, the catalyst must be reduced and oxidized by two-electrons in each half-reaction. The estimated two-electron reduction potential for the Fe^{III}_2/Fe^{II}_2 couple of **3** (-0.19 V) is out of the range required for CAT activity, and, thus, it is expected to be active through a catalytic cycle involving iron in higher oxidation state. The activity of complex **3**, and its Mn_2 analogue, toward H_2O_2 in aqueous solution was determined by volumetric measurement of evolved O_2. Figure 6(a) shows the evolution of O_2 vs. time after addition of 150 equivalents of H_2O_2 to aqueous solutions containing 3.3 mmol of **3** or [$Mn_2(5\text{-}SO_3\text{-}salpentO)(\mu\text{-}OAc)(\mu\text{-}OMe)$]$^-$. It can be seen that the diMn complex dismutates all H_2O_2 within 1 h, whereas the Fe_2 analogue requires 7.3 h to dismutate the same H_2O_2 amount. The CAT activity of the Fe_2/Mn_2 analogues was also evaluated in basic medium. After addition of Et_3N to the complex solution, the starting complexes convert into [$M_2(5\text{-}SO_3\text{-}salpentO)(\mu\text{-}O)$]$^-$. As it was described in the previous section, the reduction potential of the μ-oxo-M_2^{III} centers shifts to potentials considerably lower than those of μ-OR(OH)-M_2^{III} centers, so the catalytic disproportionation of H_2O_2 in basic medium must certainly involve higher metal oxidation states. As shown in figure

6(b), under the same experimental conditions, the μ-oxo-Mn$_2^{III}$ complex dismutates 150 eq H$_2$O$_2$ in 4 min, while the μ-oxo-Fe$_2^{III}$ analogue takes more than 7 h. Thus, in aqueous solution, **3** is about 10 times slower than the Mn$_2^{III}$ analogue, while the μ-oxo-Fe$_2^{III}$ complex is about 100 times slower than its μ-oxo-Mn$_2^{III}$ counterpart in basic medium.
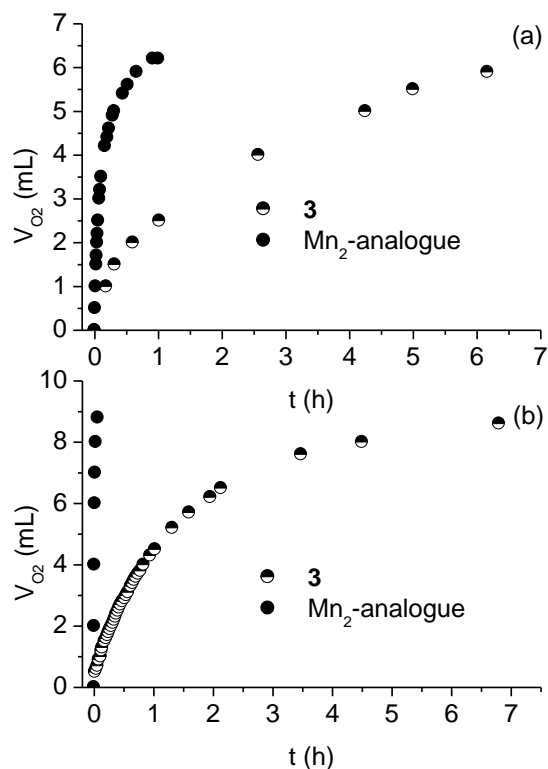
Figure 6. Volume of O$_2$ evolved from a mixture of (a) catalyst (1.1 mM) + 150 eq H$_2$O$_2$ in 3.05 mL H$_2$O. (b) catalyst (1.56 mM) + 150 eq H$_2$O$_2$ + 10 eq Et$_3$N in 3.07 mL H$_2$O. T = 298 K.

It is known that dimanganese complexes of the X-salpentOH family disproportionate H$_2$O$_2$ employing the Mn$_2^{III}$/(Mn^{IV}=O)$_2$ couple.[24] In order to obtain additional information on the Fe species involved in the H$_2$O$_2$ disproportionation in basic medium, a mixture of **3** + 150 eq H$_2$O$_2$ + 10 eq Bu$_4$NOH in DMF was monitored by resonance Raman (RR) spectroscopy. DMF was used because water or methanol did not show enhanced lines in the RR spectra. The RR spectra, obtained with 514 nm excitation, are shown in figure 7(a). In the spectrum of complex **3** in DMF the peak observed at 729 cm^{-1} may be assigned to a PhO-Fe stretching mode.[16b,25] RR spectra recorded at different times during the reaction show two additional peaks at 513 and 613 cm^{-1}. The peak at 513 cm^{-1} may be tentatively assigned to the ν_s(Fe-O-Fe) mode, whose intensity appears to be related to the presence of additional bridging groups as well as to the nature of the non bridging ligands.[14] In particular, the intensity of this mode is depressed by phenolate ligands,

and this could be the reason for its low intensity in the present case. Therefore, RR spectroscopy seems to confirm that the μ-oxo-Fe_2^{III} species could be involved in the catalytic cycle. The spectrophotometric monitoring of the reaction of the μ-oxo-Fe_2^{III} shows that the absorption band at 368 nm decreases with time during the reaction course (figure 7(b)). This indicates that, besides the intrinsic properties of the Mn/Fe complexes that determine their different activity toward H_2O_2, the lower activity of the Fe_2-catalyst is in part due to partial decomposition of the complex during the H_2O_2 disproportionation. In line with this, the peak at 614 cm^{-1} in the RR spectra of the reaction mixture may be assigned to the enhanced ν_{phO-Fe} mode of a mononuclear species formed by decomposition of the catalyst.
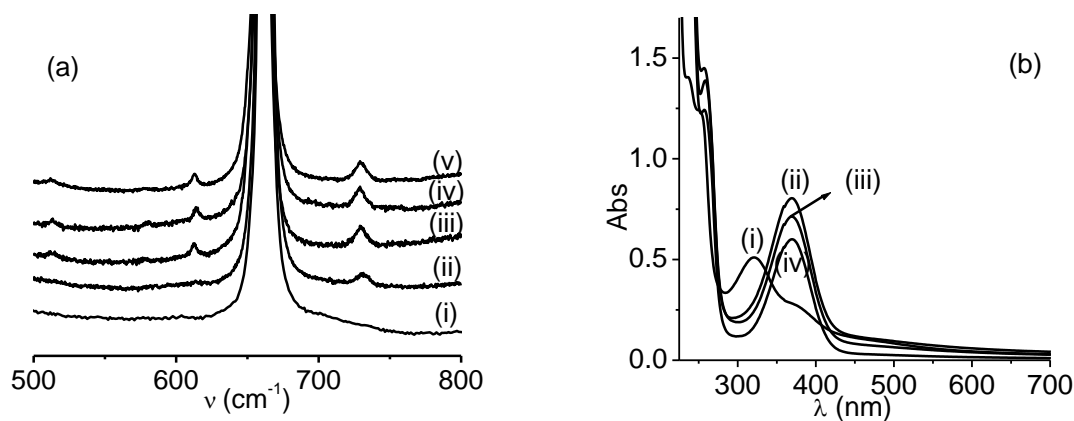

Figure 7. (a) RR spectra of solvent alone (i); a DMF solution of **3** (ii); a mixture of **3** + 150 eq H_2O_2 + 10 eq Bu_4NOH at 14 (iii), 17 (iv) and 35 min (v) after mixing. 514 nm excitation; [**3**] = 1.8 mM. (b) UV-vis spectra of 3 (i) and a reaction mixure of **3** (5.55×10^{-2} mM) + 150 eq H_2O_2 + 5 eq Et_3N, 3 min (ii), 2 h (iii) and 6 h (iv) after mixing.

Conclusions

The present results show that the length of the aliphatic chain in 5-SO_3-salpn, 5-SO_3-salpnOH and 5-SO_3-salpentOH controls the nuclearity of the iron complex affording compounds that are structurally analogous to those of Mn. 5-SO_3-salpn and 5-SO_3-salpnOH modulate the iron-centered reduction potential to values that are only 0.1 V more negative than those of their Mn counterparts and result in Fe/Mn complexes that are thermodynamically competent to disproportionate $O_2^{\bullet-}$. Therefore, **1 - 2** and their Mn analogues behave as cambialistic SOD models. However, the more distant Fe^{III}/Fe^{II} couple to the midpoint potential for $O_2^{\bullet-}$ dismutation and the lower stability of the Fe complexes toward dissociation render complexes **1 – 2** less efficient than the Mn counterpart. 5-SO_3-salpentOH affords Fe_2/Mn_2 analogues that convert into μ-oxo-M_2 species and are both competent to disproportionate H_2O_2. However,

partial decomposition of complex **3** results in a catalyst poorer than the Mn_2 counterpart. This is especially evident in basic medium where the Mn_2 catalyst shows enhanced activity and stability.

Experimental Section

General. All reagents or analytical grade chemicals were used as purchased. Solvents were purified by standard methods. The concentration of H_2O_2 stock solution was determined by iodometric titration. Disodium salts of 1,5-bis(5-sulphonatosalicylidenamino)pentan-3-ol (5-SO_3-salpentOH), 1,3-bis(5-sulphonatosalicylidenamino)propan-2-ol (5-SO_3-salpnOH) and 1,3-bis(5-sulphonatesalicylidenamino)propane (5-SO_3-salpn) were prepared by Schiff base condensation of sodium salicylaldehyde-5-sulphonate[26] and 1,5-diaminopentan-3-ol, 1,3-diaminopropan-2-ol and 1,3-diaminopropane, respectively, as previously reported.[9,12]

Physical measurements

Electronic spectra were recorded on a JASCO V550 spectrophotometer with thermostated cell compartments. IR spectra were recorded on a Perkin-Elmer Spectrum One FT-IR spectrophotometer. ESI-mass spectra were recorded on a Perkin-Elmer SCIEX 365 LCMSMS mass spectrometer. The electrospray solutions were prepared in methanol with final $\approx 10^{-5}$ M concentration and the flow rate was 5 μL min^{-1}. ^1H spectra were recorded on a Bruker AC 200 NMR spectrometer at ambient probe temperature (ca 26 ℃), with nominal operating frequency of 200.1 MHz. The electrochemical experiments were performed with a computer-controlled Princeton Applied Research potentiostat, model VERSASTAT II, with model 270/250 Research Electrochemistry Software. Studies were carried out under Ar, in water or methanol solutions using 0.1 M KNO_3 or Bu_4NPF_6, respectively, as supporting electrolyte and ~10^{-3} M of the complex. The working electrode was a Pt wire and the reference electrode was Ag/AgCl with Pt as the auxiliary electrode. Resonance Raman spectra were measured in backscattering geometry by using a confocal microscope (Olympus BX41) coupled to a single-stage spectrograph (Jobin Yvon XY 800) equipped with a liquid-nitrogen-cooled back-illuminated CCD detector and an 1800 l/mm grating. Elastic scattering was rejected with an edge filter (Semrock). The 514 nm line of a cw argon laser (Coherent Innova 70c) was focused into ca. 100 microL solution film in a rotating quartz cell using a 20x objective (20.5 mm wd, 0.35 N.A.) Spectra were acquired with laser powers of about 13mW at sample, and were processed with home-made software for baseline correction and peak determination. Spectral positions were aligned towards standard Hg and Na lamps.

Synthesis of complexes

$Na_2[Fe(5-SO_3-salpn)(H_2O)_2]OH·4H_2O$ ($1·4H_2O$). $FeCl_3·6H_2O$ (110 mg, 0.4 mmol) was added to a solution of $Na_2[5-SO_3-salpn]$ (193 mg, 0.43 mmol) in methanol (10 mL) and left to stir for 12 h. After addition of 2 mL of CH_3CN, the complex precipitated as a red-wine solid that was

filtered off, washed with ether and dried under vacuum. Yield: 110 mg (0.17 mmoles, 42%). Anal. calcd. for $C_{17}H_{19}FeN_2Na_2O_{11}S_2 \cdot 4H_2O$: C 30.7, H 4.09, N 4.21, Na 6.9%; found: C 31.02, H 3.60, N 4.25, Na 6.5%. Significant IR bands (KBr, ν cm^{-1}): ν_{OH} 3427 (broad), ν_{CH} 3045, $\nu_{C=N}$ 1623, ν_{phO} 1545, ν_{SO3} 1113/1028. UV-vis λ_{max} nm (ε M^{-1}cm^{-1}) in H_2O: 316 (5950), 513 (2270). ESI-MS (m/z, MeOH): 534 (Na[Fe(5-SO$_3$-salpn)(OH)]$^-$), 525 ([Fe(5-SO$_3$-salpn)(OMe)]$^-$), 494 ([Fe(5-SO$_3$-salpn)]$^-$).

Na$_2$[Fe(5-SO$_3$-salpnOH)(H$_2$O)$_2$]Cl·7H$_2$O (2·7H$_2$O). Na$_2$[5-SO$_3$-salpnOH] (191 mg, 0.38 mmol) and FeCl$_3$.6H$_2$O (110 mg, 0.4 mmol) were mixed in methanol (11 mL). The mixture was stirred for 12 h and a red-wine powder precipitated after slow evaporation of the solvent. The solid was collected by filtration, washed with ether and dried under vacuum. Yield: 101 mg (0.13 mmol, 34 %). Anal. Calcd. for $C_{17}ClH_{18}FeN_2Na_2O_{11}S_2 \cdot 7H_2O$: C 27.09, H 4.28, N 3.72, Na 6.1%; found: C 26.95, H 4.05, N 3.67, Na 6.2%. Conductimetric titration of **2** with AgNO$_3$ afforded 1 eq. of Cl$^-$ per mol of complex. Significant IR bands (KBr, ν cm^{-1}): ν_{OH} 3405 (broad), ν_{CH} 3091, $\nu_{C=N}$ 1630, ν_{phO} 1538, ν_{SO3} 1106/1028. UV-vis λ_{max} nm (ε M^{-1}cm^{-1}) H_2O: 310 (11175), 474 (2590). ESI-MS (m/z, MeOH): 585.7 (NaH[Fe(5-SO$_3$-salpnOH)(MeOH)(H$_2$O)]$^+$), 563.7 (H$_2$[Fe(5-SO$_3$-salpnOH)(H$_2$O)(MeOH)]$^+$).

Na$_2$[Fe$_2$(5-SO$_3$-salpentO)(μ-OAc)(μ-OH)(H$_2$O)$_2$]OH·3H$_2$O (3·3H$_2$O). A solution of Fe(OAc)$_2$ (296 mg, 1.70 mmol) in 3 mL of methanol was added to a solution of Na$_2$[5-SO$_3$-salpentOH] (500 mg, 0.94 mmol) in methanol (3 mL). The mixture was stirred for 24 h and a solid began to form slowly. After standing for 4 days, the resulting brick-red precipitate was collected by filtration, washed with cold methanol and dried under vacuum. Yield: 420 mg (0.51 mmol, 54%). Anal. Calcd. for $C_{21}H_{26}Fe_2N_2Na_2O_{15}S_2 \cdot 3H_2O$: C 30.7, H 3.92, N 3.41, Fe 13.6, Na 5.6%; found: C 30.6, H 3.60, N 4.18, Fe 12.9, Na 6.1%. Significant IR bands (KBr, ν cm^{-1}): ν_{OH} 3430 (broad), ν_{CH} 2820, 2860, 2920, 2960, $\nu_{C=N}$ 1635, ν_{Ph-O} 1537, ν_{OAc} 1427/1552, ν_{SO3} 1112/1039. UV-vis λ_{max} nm (ε M^{-1}cm^{-1}) H_2O: 220 (57300), 320 (9270), 368 (sh, 5240), 440 (broad, 2180). ESI-MS (m/z, MeOH): 683 ([Fe$_2$(5-SO$_3$-salpentO)(MeO)(OAc)]$^-$), 737 (Na[Fe$_2$(5-SO$_3$-salpentO)(MeO)$_2$(OAc)]$^-$) and 765 (Na[Fe$_2$(5-SO$_3$-salpentO)(MeO)(OAc)$_2$]$^-$).

Indirect SOD assay

The SOD activity of the complexes was assayed by measuring inhibition of the photoreduction of nitro blue tetrazolium (NBT), by a method slightly modified from that originally described by Beauchamps and Fridovich.[27] The solutions containing riboflavin (3.4 x 10^{-6} M), methionine (0.01 M), NBT (4.6 x 10^{-5} M) and complex of various concentrations were prepared with phosphate buffer (pH 7.8). The mixtures were illuminated by a regular compact fluorescent lamp with a constant light intensity at 25 ºC. The reduction of NBT was monitored at 560 nm with various illumination periods (t). Rates in the absence and in the presence of different concentrations of complex were determined and plotted vs. complex concentration. Inhibition percentage was calculated according to: $\{(\Delta Abs/t)_{without\ complex} - (\Delta Abs/t)_{with\ complex}\} \times 100 / (\Delta Abs/t)_{without\ complex}$. The IC_{50} value represents the concentration of the SOD mimic that induces a 50% inhibition of the reduction of NBT. Control experiments were performed on mixtures of

NBT + complex, riboflavin + complex, and NBT + methionine + complex, in phosphate buffer, to ensure that the complex does not react independently with any of the components of the mixture. On the basis of competition with NBT, at 50% inhibition the rates of the reactions of NBT and the mimic with $O_2^{\bullet-}$ are equal, k_{cat} [catalyst] = k_{NBT} [NBT], where k_{NBT} (pH = 7.8) = 5.94 × 10^4 M^{-1} s^{-1}.[28] Hence, the catalytic rate constant was calculated as $k_{cat} = k_{NBT}$ [NBT]/IC_{50}.

Disproportionation of H_2O_2

The H_2O_2 disproportionation catalyzed by **1**-**3** was measured by volumetric determination of the evolved O_2 from reaction mixtures in water. A round-bottom flask with a stopcock equipped gas delivery side tube connected to a gas-measuring burette (precision of 0.1 mL) was used. A closed vessel containing a solution of catalyst in water or Et₃N ([Et₃N]:[catalyst] ratios from 5:1 to 20:1) was stirred at constant temperature on a water bath. Previously thermostated H_2O_2 ([H_2O_2]:[catalyst] ratio 150:1) was injected through a silicon stopper, and the evolved dioxygen was volumetrically measured.

Acknowledgements

References

1   (a) Chang, L.; Slot, J. W.; Geuze, H. P.; Crapo J. D. *J. Cell Biol.* **1988**, *107*, 2169. (b) Barondeau, D. P.; Kassmann, C. J.; Bruns, C. K.; Tainer, J. A.; Getzoff, E. D. *Biochemistry* **2004**, *43*, 8038. (c) Edwards, R. A.; Baker, H. M.; Whittaker, M. M.; Whittaker, J. W.; Jameson, G. B.; Baker, E. N. *J. Biol. Inorg. Chem.* **1998**, *3*, 161. (d) Noodleman, L.; Lovell, T.; Han, W. G.; Li, J.; Himo, F. *Chem. Rev.* **2004**, *104*, 459.

2   (a) Bravo, J.; Mate, M. J.; Schneider, T.; Switala, J.; Wilson, K.; Loewen, P. C.; Fita, L. Proteins Struct. Funct. Bioinf. **1999**, *34*, 155. (b) Antonyuk, S. V.; Barynin, V. V. *Crystallogr. Reports* **2000**, *45*, 105. (c) Barynin, V. V.; Whittaker, M. M.; Antonyuk, S. V.; Lamzin, V. S.; Harrison, P. M.; Artymiuk, P. J.; Whittaker, J. W. *Structure* **2001**, *9*, 725.

3   (a) Ihara, Y.; Chuda, M.; Kuroda, S.; Hayabara, T. *J. Neurol. Sci.* **1999**, *170*, 90. (b) Toh, Y.; Kuninaka, S.; Mori, M.; Oshiro, T.; Ikeda, Y.; Nakashima, H.; Baba, H.; Kohnoe, S.; Okamura, T.; Sugimachi, K. *Oncology* **2000**, *59*, 223.

4   Miller, A. F. In *Handbook of Metalloproteins*; Messerschmidt, A.; Huber, R.; Wieghardt, K.; Paulos T. Eds.; Wiley and Sons: Chichester, U.K., 2001; Vol. 2, pp 668-682.

5   (a) Mukhopadhyay,S.; Mandal, S. K.; Bhaduri, S.; Armstrong, W. H. *Chem. Rev.* **2004**, *104*, 3981. (b) Wu, A. J.; Penner-Hahn, J. E.; Pecoraro, V. L. *Chem. Rev.* **2004**, *104*, 903-938. (c) Signorella, S.; Rompel, A.; Buldt-Karentzopoulos, K.; Krebs, B.; Pecoraro, V. L.; Tuchagues, J.-P.; *Inorg. Chem.* **2007**, *46*, 10864-10868. (d) Signorella, S.; Tuchagues, J.-P.; Moreno, D.; Palopoli, C. In *Inorganic Biochemistry Research Progress*; Hughes, J. G.; Robinson, A. J. Eds.; Nova Sci. Publ. Inc.: New York, 2008; pp 243.

6   (a) Riley, D. P. *Chem. Rev.* **1999**, *99*, 2573. (b) Lahaye, D.; Muthukumaran, K.; Hung, C. H.; Gryko, D.; Rebouças, J. S.; Spasojevic, I.; Batinic-Haberle, I.; Lindsey, J. S. *Biorg. Med. Chem.* **2007**, *15*, 7066. (c) Spasojevic, I.; Batinic-Haberle, I.; Stevens, R. D.; Hambright, P.; Thorpe, A. N.; Grodkowski, J.; Neta, P.; Fridovich, I. *Inorg. Chem.* **2001**, *40*, 726.

7   (a) Sjödin, M.; Gätjens, J.; Tabares, L. C.; Thuéry, P.; Pecoraro, V. L.; Un, S. *Inorg. Chem.* **2008**, *47*, 2897. (b) Groni, S.; Hureau, C.; Guillot, R.; Blondin, G.; Blain, G.; Anxolabéhère-Mallart, E. *Inorg. Chem.* **2008**, *47*,11783, and refs. cited therein.

8   Doctrow, S. R.; Huffman, K.; Marcus, C. B.; Tocco, C.; Malfroy, E.; Adinolfi, C. A.; Kruk, H.; Baker, K.; Lazarowych, N.; Mascarenhas, J.; Malfroy, B. *J. Med. Chem.* **2002**, *45*, 4549.

9   Moreno, D.; Daier, V.; Palopoli, C.; Tuchagues, J. P.; Signorella S. *J. Inorg. Biochem.* **2010**, *104*, 496.

10   (a) Deacon, G. B.; Phillips, R. J. *Coord. Chem. Rev.* **1980**, *33*, 227. (b) Nakamoto, K. *Infrared and Raman Spectra of Inorganic and Coordination Compounds*, 5th Edn.; Wiley-Interscience: New York, 1997; Part B, p 60.

11   Signorella, S.; Palopoli, C.; Daier, V.; Ghinamo, L.; Micheloud M. *EUROBIC10*, Thesaloniki, Greece, October 22-26, 2010: Abstract No 233.

12   Palopoli, C.; Bruzzo, N.; Ghinamo, L.; De Gaudio, M.; Beltramino, C.; Signorella, S. *EUROBIC10*, Thesaloniki, Greece, October 22-26, 2010: Abstract No 183.

13   (a) Ramesh, K.; Mukherjee, R. *J. Chem. Soc., Dalton Trans*. **1992**, 83. (b) Cook, D.; Cummins, D.; McKenzie, E.D. *J. Chem. Soc., Dalton Trans*. **1976**, 1369.

14   Sanders-Loehr, J.; Wheeler, W. D.; Shiemke, A. K.; Averill, B. A.; Loehr, T. M. *J. Am. Chem. Soc.* **1989**, *111*,8084.

15   LaMar G. N. In *NMR of Paramagnetic Molecules, Principles and Applications*; LaMar, G. N.; Worrocks, W. D.; Holm, R. H. Eds.; Academic Press: New York, 1973, ch 3.

16   (a) LaMar, G. N.; Eaton, G. R.; Holm, R. H.; Walker, F. A. *J. Am. Chem. Soc*. **1973**, *95*, 63. (b) Pyrz, J. W.; Roe, A. L.; Stern, L. J.; Que, Jr., L. *J. Am. Chem. Soc.* **1985**, *107*, 614.

17   Gelasco, A.; Kirk, M. L.; Kampf, J. W.; Pecoraro, V. L**.** *Inorg. Chem.*, **1997**, *36*, 1829.

18   Aimscough, E. W.; Brodie, A. M.; Plowman, J. E.; Brown, K. L.; Addison, A. W.; Gainsford, A. R. *Inorg. Chem*. **1980**, *19*, 3655.

19   Armstrong, W. H.; Spool, A.; Papaefthymiou, G. C.; Frankel, R. B.; Lippard, S. J *J. Am. Chem. Soc.* **1984**, *106*, 3653.

20   Mukherjee, R. N.; Abrahamson, A. J.; Patterson, G. S.; Stack, T. D. P.; Holm, R. H. *Inorg. Chem.* **1988**, *27*, 2137.

21 Batinic-Haberle, I.; Spasojevic, I.; Hambright, P.; Benov, L.; Crumbliss, A. L.; Fridovich, I. *Inorg. Chem.* **1999**, *38*, 4011.

22 Vance, C. K.; Miller, A. F.; *J. Am. Chem. Soc.* **1998**, *120,* 461.

23 Stassinopoulos, A.; Mukerjee, S.; Caradonna, J. P. In *Mechanistic Bioinorganic Chemistry*; Thorp, H. H.; Pecoraro, V. L. Eds; Advances in Chemistry Series, 246; ACS: Washington DC, 1995; pp 83-120.

24 (a) Moreno, D.; Palopoli, C.; Daier, V.; Shova, S.; Vendier, L.; González Sierra, M.; Tuchagues, J.-P.; Signorella, S. *Dalton Trans.* **2006**, 5156. (b) Biava, H.; Palopoli, C.; Shova, S.; De Gaudio, M.; Daier, V.; González-Sierra, M.; Tuchagues, J.-P.; Signorella, S. *J. Inorg. Biochem.* **2006**, *100,* 1660. (c) Daier, V.; Biava, H.; Palopoli, C.; Shova, S.; Tuchagues, J.-P.; Signorella, S. *J. Inorg. Biochem.* **2004**, *98*, 1806. (d) Palopoli, C.; González-Sierra, M.; Robles, G.; Dahan, F.; Tuchagues, J.-P.; Signorella, S. *J. Chem. Soc., Dalton Trans.* **2002**, 3813. (e) Palopoli, C.; Chansou, B.; Tuchagues, J.-P.; Signorella, S. *Inorg. Chem.* **2000**, *39*, 1458.

25 Gonçalves, N.S.; Rossi, L. M.; Noda, L. K.; Santos, P. S.; Bortoluzzi, A. J.; Neves, A.; Vencato, I. *Inorg. Chim. Acta* **2002**, *329*, 141.

26 (a) Berry, K. J.; Moya, F.; Murray, K. S.; v. d. Bergen, A. M. B.; West, B. O. *J. Chem. Soc., Dalton Trans.* **1982**, 109. (b) Botsivali, M.; Evans, D. F.; Missen, P. H.; Upton, M. W. *J. Chem. Soc., Dalton Trans.* **1985**, 1147.

27 Beauchamps, C.; Fridovich, I. *Anal. Biochem.* **1971**, *44*, 276.

28 (a) Durot, S.; Policar, C.; Cisnetti, F.; Lambert, F.; Renault, J.-P.; Pelosi, G.; Blain, G.; Korri-Youssoufi, H.; Mahy, J.-P. *Eur. J. Inorg. Chem.* **2005**, 3513. (b) Liao, Z. R.; Zheng, X. F.; Luo, B. S.; Shen, L. R.; Li, D. F.; Liu, H. L.; Zhao, W. *Polyhedron* **2001**, *20*, 2813.